ORIGINAL ARTICLE

Impact of increased outer wall rotation on convection in a vertical annulus with a stationary heated inner cylinder

K. Pillai Sidharth[1] | Mattacaud R. Rajkumar[2] |
V. K. Chithrakumar[1] | Godson L. Asirvatham[3] |
Ali Cemal Benim[4] | Somchai Wogwises[5]

[1]Advanced Thermo Fluid Research Lab, Department of Mechanical Engineering, College of Engineering Trivandrum, APJ Abdul Kalam Technological University, Thiruvananthapuram, Kerala, India

[2]Department of Mechanical Engineering, Rajiv Gandhi Institute of Technology, APJ Abdul Kalam Technological University, Kottayam, Kerala, India

[3]Department of Mechanical Engineering, Karunya University, Coimbatore, Tamil Nadu, India

[4]Centre of Flow Simulation (CFS), Faculty of Mechanical and Process Engineering, Duesseldorf University of Applied Sciences, Düsseldorf, Germany

[5]Fluid Mechanics, Thermal Engineering and Multiphase Flow Research Lab (FUTURE), Department of Mechanical Engineering, Faculty of Engineering, King Mongkut's University of Technology, Bangkok, Thailand

Correspondence
Mattacaud R. Rajkumar, Department of Mechanical Engineering, Rajiv Gandhi Institute Of Technology, APJ Abdul Kalam Technological University, Kottayam, Kerala, India.
Email: rajkumar@cet.ac.in

Abstract

The interplay of centrifugal and buoyant forces on convective heat transfer in a vertical annulus formed by rotating adiabatic outer cylinder and stationary heated inner cylinder has been experimentally and numerically investigated. Experiments were performed for rotational speeds corresponding to the rotation parameter ζ in the range of $527 \leq \zeta \leq 2860$, maintaining the heat flux of the heated stationary inner cylinder as $80 \, \text{W/m}^2$, for radius ratio (η) and aspect ratio of the vertical annulus being 0.614 and 0.052, respectively. The problem was investigated numerically using the commercial computational fluid dynamics package, ANSYS CFX. The numerical methodology has been validated by comparing the numerically predicted average surface Nusselt number with experimentally obtained values. The comparison revealed an enhancement of the thermal performance of the heated stationary inner cylinder in the range $527 \leq \zeta \leq 1190$ due to the increase in turbulence intensity towards the heated inner cylinder. However, when the rotation parameter was increased further in the range $1190 \leq \zeta \leq 2860$, the thermal performance of the stationary heated inner cylinder showed only marginal

improvement. The aforementioned thermal behavior of the inner heated stationary cylinder has been explored based on the flow statistics gathered from the numerical simulations.

1 | INTRODUCTION

The study of heat transfer in vertical/horizontal annuli with either rotating or stationary wall(s) was motivated by the fact that these structures are often encountered in many engineering application devices, such as turbomachinery, rotating tube heat exchangers, and electric motors. The heat transfer in the above-mentioned devices is influenced by the interesting flow structures that evolve in their annular gaps.[1,2] Therefore, the study pertaining to the flow structures has been thought-provoking to many researchers. The stability of the flow structure in the annular gap is highly influenced by the velocity profile in the radial direction. Based on the velocity profile in the annular gap, vertical/horizontal annuli can be classified into two configurations: (i) Configuration A: inner cylinder rotating and outer cylinder stationary (electric motors) and (ii) Configuration B: outer cylinder rotating and inner cylinder stationary (BLDC Motor).

Configuration A: Early investigation pertaining to this geometry was numerically simulated by El-Shaarawi et al.[3] The authors, using a finite difference scheme, studied natural convection flow in this annuli while subjecting it to two different cases: a radially increasing temperature field and a radially decreasing temperature field. Their study revealed that heating of the inner cylinder has a stabilizing effect on the flow structure, while the flow is destabilized in the case of a heated outer cylinder. Fenot et al.[4] conducted a comprehensive review of the flow structure in the concentric annulus. The authors reviewed various configurations of flow and thermal boundary conditions in concentric annuli and reported on the multitude of influential factors that influence the flow cases. After this extensive survey based on 71 research articles, Fenot et al. pointed out how contradictory and far less understood the conclusions are in Taylor–Couette–Poiseuille flow cases, essentially due to the different influential parameters guiding the flow. This has led to disparities in the results of various cases. The authors concluded that questions relating to flow characteristics and thermal performances in many such configuration devices are still not clearly understood. This has encouraged many researchers to continue the work on this configuration as detailed below.

Yoshikawa et al.[5] performed a linear stability analysis of flow confined in a concentric cylindrical annulus having a fixed radius ratio. The system was subjected to a radial temperature gradient (both cases of inner and outer cylinders maintained separately at higher temperatures), without varying the Prandtl number. It was observed that compared to the stationary Taylor modes, spiral vortices having a larger wavelength, started traveling in the azimuthal direction due to flow destabilization caused by radial temperature gradient. The analysis was able to provide better quantitative explanations for the earlier experimental

investigations of similar configurations thereby signifying the importance of numerical simulations in obtaining quantitative data. Experimental and numerical (DNS) investigations of flow in a differentially rotating cylindrical annulus with a radially decreasing temperature gradient for a wide range of temperature differences $(0 < Gr < 2500)$ and rotation rate $(0 < Ta < 100)$ were performed by Guillerm et al.[6] The results of the linear stability analysis and DNS were found to agree well with the experimental results. At higher speeds of rotation higher heat transfer rates were observed which was attributed to the presence of secondary vortices in the flow field. Sankar et al.[7] numerically investigated natural convection in a vertical annular enclosure in which the bottom wall of the annulus was uniformly heated while the top wall was thermally insulated. The authors considered two different thermal boundary conditions, viz: the inner and outer walls being linearly heated, linearly heated inner wall and cooled outer wall. Their study revealed that the flow pattern and distribution of temperature in the enclosure were significantly influenced by the aforementioned boundary conditions.

The role of axial boundary conditions (both periodic and no-slip boundary conditions) on heat transfer and onset of turbulence in a vertical annulus with a radially decreasing temperature gradient was numerically investigated by Lopez et al.[8] They proposed a simple criterion that is independent of the Prandtl number to check the validity of an infinite-cylinder assumption even beyond the laminar regime. This helped to greatly simplify the theoretical treatment of the problem. It was concluded that the instabilities in the flow were driven by two physical mechanisms: (1) Changing axial velocity profile generated by the thermal buoyancy and (2) Centrifugal instabilities promoted by the inner-cylinder rotation. Schneider et al.[9] performed large-eddy simulations (LES) for understanding the flow and heat transfer in the annular gap between two concentric cylinders. The outer cylinder is adiabatic while the inner cylinder is heated with the application of constant heat flux. The study was done for two values of rotation numbers (0.21 and 0.86) for the inner cylinder rotation and a constant bulk flow Reynolds number value of 9000. The Results reported by them provided useful contributions to the very limited literature on the numerical study of heated turbulent flows destabilized by rotation, and serve as a benchmark to aid in the development and validation of turbulence closures for many engineering applications. Nouri-Borujerdi and Nakhchi[10] conducted experimental studies on heat transfer enhancement for annular flow with outer grooved cylinders considering parameters like Taylore number, Groove aspect ratio $0 \leq \frac{b}{c} \leq 2$, number of grooves and different wall temperatures. Their study suggested that the thermal entrance length gets reduced by 17% and heat transfer enhances with effectiveness of 1.33 for a groove aspect ratio of 2.

Configuration B: Even though extensive research has been done by many investigators on the flow dynamics and thermal characteristics of concentric vertical/horizontal annulus, studies pertaining to concentric annuli with outer wall rotating and inner wall stationary and heated/unheated were scarce. The geometry mentioned above has applications in rotating reactors,[11] brushless DC motors used in electric vehicles, fans, and mechanical drives.[12,13] Few research done on this configuration to delineate the flow and thermal field are described here. The effect of forced flow caused by the rotating outer cylinder on the two-dimensional (2D) natural convection's heat transfer and fluid flow characteristics within a horizontal annulus was numerically analyzed by Yoo.[14] The flow patterns were significantly influencing the overall heat transfer with respect to the angular velocity of the cylinder. According to the number of eddies formed, flow patterns are divided into three categories: two-, one-, and no-eddy flows. Overall heat transfer at the wall is rapidly decreased, as the Reynold number approaches the transitional Reynolds number between two- and one-eddy flows. Lee et al.[15] performed LES to

analyze the effect of outer wall rotation on heat transfer in an imposed annular turbulent flow situation. Their simulation could predict a deterioration in turbulence intensity near the outer rotating wall with a subsequent increase in intensity close to the heated wall resulting in improved heat transfer from the heated inner cylinder. LES was carried out by Hadziabedic et al.[16] to explore the turbulence parameter in a horizontal annulus with an imposed axial flow. They delineated that the nondimensional rotational rate (ratio of circumferential velocity to axial bulk velocity) has a major influence on mean flow turbulent statics and eddy structures. It can be seen that research done for understanding the flow structures and thermal characteristics of such types of configurations is not sufficient and therefore calls for further investigations.

In addition to the above-mentioned configurations, many interesting geometric configurations have also been considered in this massive research area. Ejaz et al.[17] conducted an experimental study on heat transfer in a vertical annulus with a rotating inner cylinder. The outer cylinder was stationary and the bottom end of the annulus was heated. They found that the influence of the Rayleigh number on heat transfer (Nu) was significant only at lower values of rotational Reynolds number and became independent at higher speeds of rotation. Various interesting studies of geometric configurations having enclosed bodies subjected to rotation can be found; a few of them are cited here.[18,19]

Recently, Chithrakumar et al.[20] conducted an experimental and numerical investigation to examine the coaction of buoyancy and centrifugal forces in a vertical concentric annulus geometrically identical to Configuration B. In this study, results were presented for rotation parameter range $0 \leq \zeta \leq 527$ (low rotational speeds). They reported a progressive improvement in heat transfer up to a rotational speed corresponding to rotation parameter $\zeta = 212$ and a further increase in rotation parameter resulted in a consequential drop in the rate of heat transfer. The speed of the rotation of the outer cylinder was limited to 460 rpm. The unique behavior in heat transfer rate was attributed to the complex flow structures that influenced the mass flow rate through the annulus.

Engineering application devices like BLDC motors have a geometric configuration similar to Configuration B where the inner cylinder is stationary and heated while the outer cylinder is rotating. These BLDC motors often operate at higher rotational speed and are mostly air-cooled. Therefore a better understanding of the heat transfer mechanism is of at most importance for their efficient operation. The influence of higher rotational speeds on flow structures and the heat transfer rate is expected to be stronger, due to the dominating centrifugal forces that will eventually result in modifying the flow structure and leading to improved heat transfer. In adherence to this practicality, the primary focus of this study is to perform combined experimental and numerical investigations to realize thermal performance and flow structures developed in such a type of configuration while operating at higher rotational speeds in the range of rotation parameters, $527 \leq \zeta \leq 2860$.

2 | EXPERIMENTAL SETUP

The schematic diagram representing the experimental setup is depicted in Figure 1. It consists of two concentric cylinders aligned vertically. The inner hollow cylinder is made of polished copper while the outer cylinder is made from transparent acrylic glass. The outer diameter and height of the inner copper tube are 51 mm and 620 mm, respectively. The thickness of the inner tube is 2 mm which will result in negligible radial conduction losses. The inner diameter of the
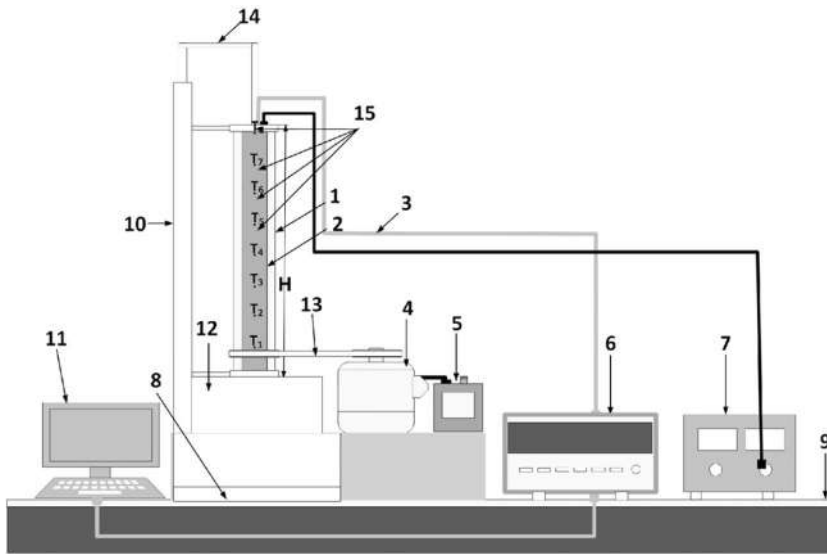
FIGURE 1 Schematic of the experimental setup. (1. Rotating outer cylinder, 2. Heated inner cylinder, 3. Thermocouple wires, 4. Three phase AC motor, 5. Variable frequency drive, 6. Data acquisition system, 7. DC power supply, 8. Opening, 9. Optical bench, 10. Frame, 11. Computer, 12. Plenum, 13. Belt drive, 14. Adjustable clamp holding the heater, 15. Thermocouple positions.)
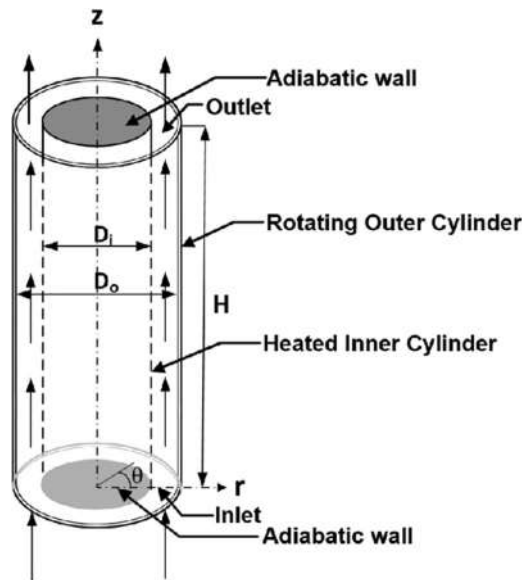

FIGURE 2 Schematic of the numerical model

outer cylinder is 83 mm, with a height the same as the inner cylinder and having a thickness of 5 mm. The schematics of the resultant annuli is shown in Figure 2. It is worth mentioning here that, the aforesaid geometrical dimensions result in an annular gap with $\eta = 0.614$, which corresponds to a moderate gap annulus ($0.584 \leq \eta \leq 0.807$).[21]

The inner copper tube is subjected to a constant heat flux of $80 \, \text{W/m}^2$ by inserting a cartridge heater from the top. The top end of the heater along with the heated inner cylinder is insulated by placing a ceramic bush with an outer dimension the same as the outer diameter of the inner cylinder. Also, the outer surface of the heated inner cylinder (copper tube) was polished $(\varepsilon = 0.02)$[22] to reduce the surface radiation effects. Copper tubes along with cartridge heater and ceramic bush are assembled and fixed to a frame from the top. Proper alignment of the inner cylinder and the outer enclosure is significant as it will significantly affect the heat transfer parameters.[23] The frame is provided with a mechanism for keeping the assembly in vertical alignment. The bottom face of the assembly is insulated by inserting a Teflon rod and this rod is then attached to the frame to act as a support to the assembly. The diameter of the Teflon rod is identical to the copper tube's outer diameter. A regulated DC power source (Aplab India Ltd) supplied to the cartridge heater regulated the heat input.

At the top and bottom ends, nylon bearings (one on each end) were attached to mount the outer cylinder in the frame, facilitating the smooth rotation of the cylinder and preventing it from undergoing any axial movement. Brackets are provided to act as support for the bearings to pitch down the axial movement that may occur during the rotation of the outer cylinder and they are attached to the frame of assembly (see Figure 1). The bottom of the outer rotating cylinder is provided with a nylon pulley. Another pulley is mounted on a three-phase squirrel cage induction motor (ABB India Ltd) which rotates the outer cylinder using an open belt drive. The two pulleys were having a 150 mm separation between them. The motor speed is varied by connecting to a variable frequency drive (Fuji Electric). The radial offset of the rotating outer cylinder was monitored by a dial gauge and the eccentricity was found to be within ± 5 microns. The disturbances caused by the surroundings at the inlet of the annulus is suppressed by attaching a plenum at the bottom. Measurement of velocity field at various points in the inlet of the annulus has been done using a hot wire anemometer.

Along the heated inner cylinder surface, calibrated 16 T-type thermocouples are positioned in pairs diametrically opposite to each other. Thermocouples were calibrated using a dry-block calibrator. The calibration process involves heating the dry-block calibrator to 30°C. Next, the free end (cold junction) of the thermocouple is connected to the 20-channel data acquisition system (HIOKI E. E. Corporation). At this stage, the DAQ resistance is 0 mV because both the junctions were at the same temperature. The hot junction of the thermocouple is now immersed in the well of the calibrator. When the voltage reading in the DAQ approaches a stable value, voltage is recorded. The dry bulb temperature is increased to 35° and again the temperature is recorded. The process is repeated by 5°C increments in temperature, correspondingly recording the voltage until a temperature of 60°C is reached. (The maximum temperature encountered in the study is 55°C). After all the measurements have been taken, the voltage for the thermocouple at room temperature is measured. The voltage corresponding to the room temperature is added to the previously gathered recorded voltages. A curve fitting method is used to fit a line to the recorded data. Since the range of temperature is very small (only up to 60°C), a linear fit is obtained. The in-site voltage from the actual measurement from the thermocouple is noted and the temperature corresponding to this voltage is retrieved from the fitted curve.

All 16 thermocouples were placed equidistantly in the axial direction (z-direction). To ensure that the thermocouple locations do not affect the flow field in the annulus, they were placed on the inner surface of the heated cylinder by machining internal longitudinal grooves along the axial direction. Also, the other ends of the thermocouples are taken out from the inner cylinder through the top face. Thermocouples are attached to the respective locations

FIGURE 3 Photograph of the experimental setup [Color figure can be viewed at wileyonlinelibrary.com]

using thermobond (Fabricka India Ltd)—a highly conducting cement. The fluid temperature at the annular exit was measured by four sheathed thermocouples (stainless steel) arranged equidistantly along the circumference at the exit. The temperature at the inlet section of the annulus was measured with two thermocouples (T-type) located in the plenum. All thermocouples are linked to a wireless data acquisition system (HIOKI E. E. Corporation). The optical bench on which the entire setup is mounted with vibration isolators serves as a reference plane for ensuring the verticality of the assembly. The photograph in Figure 3 (Refer Figure 1 for various components marked) shows the final test assembly.

3 | DATA REDUCTION

Sixteen thermocouples were used to estimate the average temperature rise of inner stationary heated cylinder as in Equation (1)

$$\Delta T_{\text{avg}} = \frac{\Sigma_{j=1}^{16} T_j}{16} - T_{\text{f}},\tag{1}$$

$$T_{\text{f}} = \frac{T_{\text{b}} + T_{\text{a}}}{2}.$$

T_{b} is the bulk fluid temperature evaluated at the outlet of the annulus.
The rotational Reynolds number (Re_{Ω}) is calculated by

$$Re_{\Omega} = \frac{\Omega r_{\text{o}} d}{\upsilon}.\tag{2}$$

Average surface heat transfer coefficient,

$$h_{\text{avg}} = \frac{Q}{A\Delta T_{\text{avg}}},\tag{3}$$

where the area A and input heat flow rate Q is calculated from,

area $A = 2\pi r_i H,$

input heat $Q = VI,$

where V and I represent the measured input voltage and current to the heater element.
Average surface Nusselt number,

$$Nu_{\text{avg}} = \frac{h_{\text{avg}} d}{\lambda_f} \tag{4}$$

4 | NUMERICAL METHODOLOGY

4.1 | Governing equations

An incompressible flow with constant material properties is assumed, as the constancy of the thermophysical quantities may be considered to be a valid assumption in the temperature range encountered in the present study. The effect of buoyancy is incorporated through the Boussinesq approximation. Within the range of considered rotation flow parameters, the flow is fully turbulent. The turbulence is treated within the framework of the Reynolds-averaged Navier–Stokes (RANS) approach.[24] Denoting the time-averaged velocity, pressure, temperature, and static enthalpy by overbars ($\bar{u}_i, \bar{p}, \bar{T}, \bar{h}$) and the fluctuating velocities in the sense of a Reynolds decomposition by primes (u_i'), the time-averaged (RANS) differential balance equations for mass, momentum, and energy in the stationary frame, as formulated by the applied CFD software ANSYS CFX[25] are provided below,

$$\frac{\partial \bar{u}_i}{\partial x_i} = 0, \tag{5}$$

$$\frac{\partial (\rho u_i u_j)}{\partial x_j} = -\frac{\partial \bar{p}}{\partial x_i} + \frac{\partial}{\partial x_j}\left(\mu \frac{\partial \bar{u}_i}{\partial x_j}\right) + \frac{\partial \left(-\rho \overline{u_i' u_j'}\right)}{\partial x_j} + \rho g_i \beta (\bar{T} - T_{\text{ref}}), \tag{6}$$

$$\frac{\partial (\rho \bar{u}_j \bar{h})}{\partial x_j} = \frac{\partial}{\partial x_j}\left((\lambda + \lambda_t)\frac{\partial \bar{T}}{\partial x_j}\right), \tag{7}$$

where ρ, μ, λ, g_i denote the density, molecular viscosity, molecular thermal conductivity, the gravitational acceleration, respectively, as β and T_{ref} stand for the thermal expansion coefficient and the reference temperature associated with the Boussinesq approximation used to model the gravity term. The term $-\rho \overline{u_i' u_j'}$ denotes the Reynolds stress tensor. The turbulence kinetic energy (k) is by definition related to the trace of the Reynolds stress tensor by

$$k = \frac{1}{2}\overline{u_i' u_i'} \tag{8}$$

Within the framework of the applied Reynolds Stress Model (RSM), a modeled transport equation for each of the six independent components of the Reynolds stress tensor is solved. By

this feature, RSM is more accurate than the turbulent viscosity models in capturing the non-isotropic turbulence structures that are predominant in strongly rotating flows.[26,27] The modeled transport equation[25] for the Reynolds stresses is provided below

$$\frac{\partial}{\partial x_k}\left(\bar{u}_k \rho \overline{u_i' u_j'}\right) = -\rho \overline{u_i' u_k'} \frac{\partial \bar{u}_j}{\partial x_k} - \rho \overline{u_j' u_k'} \frac{\partial \bar{u}_i}{\partial x_k} - \frac{2}{3}\beta' \omega k \delta_{ij} + \phi_{ij} + P_{ij,b}$$
$$+ \frac{\partial}{\partial x_k}\left(\left(\mu + \frac{\mu_t}{\sigma_k}\right)\frac{\partial \overline{u_i' u_j'}}{\partial x_k}\right)$$

(9)

where $\sigma_k = 1$, while $P_{ij,b}$ represents the turbulence production due to buoyancy and ϕ_{ij} denotes the pressure–strain correlation.[25] For the closure, the specific turbulence dissipation rate omega (ω) is needed, which is again obtained by solving its modeled transport equation[25] as given below:

$$\frac{\partial(\rho \bar{u}_j \omega)}{\partial x_j} = \frac{\partial}{\partial x_j}\left(\left(\mu + \frac{\mu_t}{2}\right)\frac{\partial \omega}{\partial x_j}\right) + \frac{5}{9}\rho \frac{\omega}{k} P_k + P_{\omega b} - 0.075\rho \omega^2,$$

(10)

where $P_k, P_{\omega b}$ represent the turbulence production by the mean strain and buoyancy, respectively. The turbulent viscosity, μ_t, which appears in the above equations (Equations 6 and 9) is obtained from

$$\mu_t = C\rho \frac{k}{\omega},$$

(11)

where C is an empirical coefficient that approaches unity for high turbulence Reynolds numbers.

With Equations (8)–(11) the Reynolds stress components can be obtained, through which the time-averaged momentum equations (Equation 6) are closed in the sense of an omega-based RSM.

Although the RSM is applied to close the momentum equations, the energy equation is not closed by solving the transport equations for the Reynolds fluxes ($-\rho \overline{u_i' h'}$) as this approach may increase the numerical instability and, thus, not incorporated in the standard solution procedure of the used software. Instead, in closing the energy equation (Equation 7) the Reynolds fluxes are obtained based on the turbulent viscosity and gradient diffusion concept, leading to the following expression for the turbulent thermal conductivity (λ_t)

$$\lambda_t = \frac{\mu_t}{Pr_t/c_p},$$

(12)

where c_p and Pr_t denote the isobaric specific heat capacity and the turbulent Prandtl number, respectively ($Pr_t = 0.9$ is assumed).

Closing the present outline on the applied mathematical modeling, the validity of the Boussinesq approximation[28] applied to model, the effect of buoyancy shall be checked (resulting in the replacement of the gravity term ρg_i in the momentum equation, Equation 2, by $\rho g_i \beta(\bar{T} - T_{ref})$ assuming constant density). The validity of the Boussinesq approximation has

been detailed in the literature.[29,30] According to the investigations, the Boussinesq approximation remains valid for $\beta \Delta T \leq 0.12$, where ΔT denotes the span of the prevailing temperature variation. In the present work, the maximum temperature range encountered is $301.15\,\text{K} \leq T \leq 331.14\,\text{K}$ for a rotation parameter of $\zeta = 527$ with an average bulk fluid temperature of 304.68 K, resulting in $\beta \Delta T = 0.09$. This confirms the validity of the Boussinesq approach used in modeling buoyancy, in the present work.

4.2 | Boundary conditions

The solution of the above coupled nonlinear partial differential equations rely on the boundary conditions. The main solution domain, that is, the annular gap between the concentric cylinders is enclosed by four boundaries. These are the inner and outer cylinder walls as well as the openings on both ends of the gap, which allow through-flow of air, and, thus, act as inlet and outlet boundaries after the onset of natural convection.

The openings at both ends of the annular gap are defined as pressure boundary conditions, prescribing the ambient static pressure at these boundaries. For the velocity components, a zero normal gradient condition is assumed. The latter is also assumed for the temperature and turbulence quantities in the case of outflow. In the case of inflow, the ambient temperature is prescribed as the boundary condition for the energy equation, while assumed values are prescribed for turbulence quantities that are derived assuming a turbulence intensity of 5% (based on the measurements) and length scale proportional to the hydraulic diameter, along with the assumption of isotropic turbulence.

On the cylinder walls, the no-slip condition holds for the momentum equations, which means that all velocity components are equal to zero, except the circumferential component of the velocity on the outer, rotating cylinder, which is equal to the rotational speed of the outer cylinder. The thermal boundary condition on the inner cylinder wall is a prescribed heat flux of $80\,\text{W/m}^2$, while the outer cylinder wall is assumed to be adiabatic.

For enabling more physically realistic inflow and outflow conditions through the annular gap (instead of obeying the zero normal gradient condition) the annular domain was extended on both sides beyond its physical length. This resulted in the above-mentioned pressure boundaries being not positioned at the physical ends of the annular gap but at some distance. The extension on the outlet side was especially important due to the occurrence of local recirculation zones, necessitating that the outlet boundary is placed sufficiently downstream. These extensions of the inner and outer walls into the air domain resulted in additional boundaries that were modeled as slip boundaries. In this context, it is important to mention that for problems of such nature, the need for extending the computational domain at the inlet and the exit has been well-documented in earlier literature.[31–33] To ensure that the recirculation zone was completely captured by the computational domain, the exit of the domain was extended by different percentages of the annulus height and the streamlines at the exit of the annulus were plotted. The boundary conditions at all the surfaces of the extended domain (both at inlet and exit of the annulus) were defined as opening (slip boundaries) to capture the recirculation effects.

The streamlines plotted in Figure 4 for the highest rotation parameter considered in the study indicate that a 50% extension of the computational domain ensured no backflow existed at the extended domain exit. Thereafter the above said pressure boundary condition (static pressure equated to atmospheric pressure) was implemented at the outlet of the extended
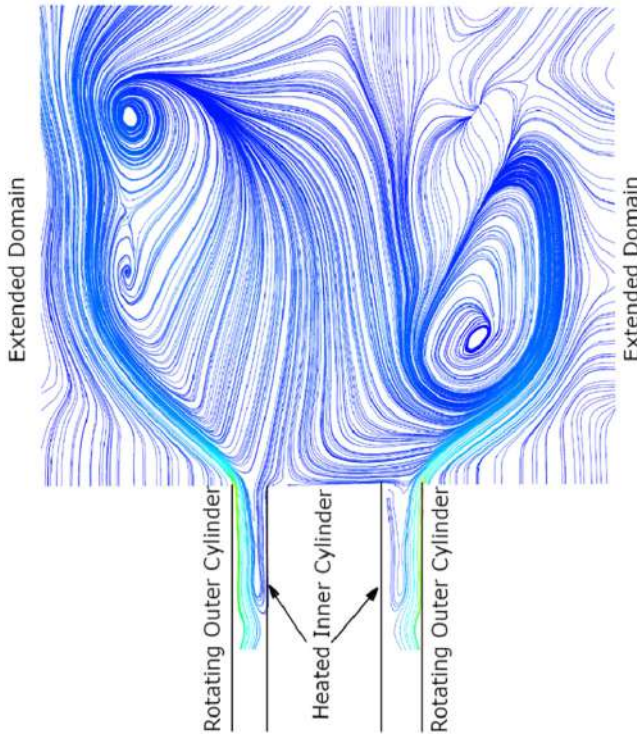
FIGURE 4 Streamlines at annulus exit with extended domain ($\eta = 0.614$, $\zeta = 2860$, $q = 80\,\text{W/m}^2$) [Color figure can be viewed at wileyonlinelibrary.com]

domain. In the present study, 50% domain extension at the annulus inlet and exit gave close agreement between the numerically predicted and experimentally measured average surface temperature of the heated inner cylinder.

The boundary conditions can be mathematically written as:

$$u = v = w = 0,\, -\lambda\frac{\partial T}{\partial n} = 80\,\text{W/m}^2 \text{ @ } r = r_\text{i}, \tag{13}$$

$$u = v = 0,\, w = r_\text{o}\Omega_\text{o},\, \frac{\partial T}{\partial n} = 0 \text{ @ } r = r_\text{o}, \tag{14}$$

$$p_\text{static} = p_\text{a},\, T = T_\text{a} \text{ @ } z = z_{d,\text{in}}, \tag{15}$$

$$p_\text{static} = p_\text{a} \text{ @ } z = z_{d,\text{out}}. \tag{16}$$

4.3 | Meshing and solver settings

Commercial meshing software ICEM CFD[34] was used to discretize the 3D computational domain into structured hexahedral cells as shown in Figure 5. To capture the value of field variables in the near-wall region, a highly refined mesh was required. This constraint was overcome by the use of a wall function approach,[35] which enables the use of a relatively coarser near-wall refinement. This may sometimes result in inconsistencies depending on the value of
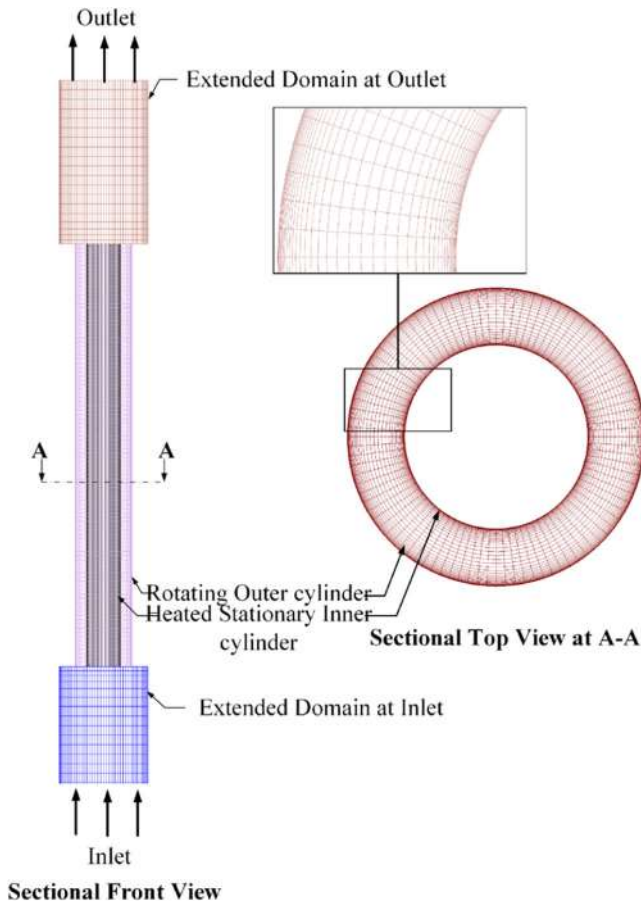
FIGURE 5 Computational domain and grid [Color figure can be viewed at wileyonlinelibrary.com]

wall Y^+ (nondimensional wall distance of the next to wall cells) along the surface of the rotating cylinder. The use of an ω-based turbulence model in ANSYS CFX (scalable wall function with automatic wall treatment) allowed the use of an arbitrarily fine mesh that can have a consistent Y^+ insensitive mesh refinement. This enables us to have a safe Y^+ value ≤ 100 which was maintained by mesh refinement.

The hard coupled solver employed Rhie–Chow pressure interpolation algorithm[25,36] to establish pressure velocity coupling. A second-order upwind scheme was used to model the convection term. The high-resolution scheme[25] available in ANSYS CFX was used to model the transport equations of the Reynolds stress model. Convergence was ensured when the residual value reached below 10^{-5}.

Based on the 50% extension of the channel height, a grid convergence study was conducted for two rotation parameters and is summarized in Table 2. As indicated in Table 2 the optimum grid size for computation corresponding to rotation parameter $\zeta = 976$ was 2,865,584 cells. However, at a higher rotation parameter of $\zeta = 2216$, it was found that the optimum grid size for this rotation parameter was 5,995,934 cells as illustrated in Table 2.

5 | RESULTS AND DISCUSSIONS

5.1 | Uncertainty analysis

The propagation of uncertainty in the independent parameters to the dependent parameters was estimated based on the method proposed by Kline and McClintock.[37,38] The independent parameters encountered in the study are geometrical dimensions, the surface temperature of heated inner cylinder, voltage, current and rotational speed of the outer cylinder. The uncertainties in the independently measured parameters mentioned above are obtained either from manufacturer specification or calibration of the instrument. The propagation of uncertainties in the aforementioned parameters to the dependent parameters, heat transfer rate (Q), average heat transfer coefficient (h_{avg}), average Nusselt number (Nu_{avg}), and rotational Reynolds number (Re_Ω) are calculated using Equation (17). The uncertainty estimation illustrated in Table 1 for heat flux $q = 80\,\text{W/m}^2$ and corresponding to rotational parameters $\zeta = 527$ and $\zeta = 1190$ shows that estimated uncertainties are well below 3.0%, thereby establishing the authenticity of the measurement techniques. Also, uncertainty estimations conducted for other rotation parameters were found to be below 3.0%

$$\sigma_R = \sqrt{\pm\left\{\Sigma_{i=1}^{n}\left[\left(\frac{\partial R}{\partial X_i}\right)^2 \sigma_{X_i}^2\right]\right\}}. \tag{17}$$

5.2 | Experimental and numerical results

Experiments were conducted for rotation parameters in the range of $527 \leq \zeta \leq 2860$ and the results are shown in Figures 6 and 7. As evident from Figure 7 that when the rotation parameter is increased from $\zeta = 527$, a sharp increase in heat transfer rate is observed from the heated inner cylinder and this heat transfer behavior is followed up to a rotation parameter value of about $\zeta = 1190$ (an overall increase of around 36%). Thereafter, the increase in heat transfer rate from the heated inner cylinder was marginal up to the rotational parameter value of $\zeta = 2860$ (an overall 5% increase).

Initially to validate the numerical methodology the numerically obtained surface temperature of the heated inner cylinder was compared with the experimentally measured temperature at identical locations and this result for rotation parameter $\zeta = 743$ is depicted here in Figure 6. Similar results were gathered for other rotation parameters but not shown here for brevity. It is evident from Figure 6 that the results compare well establishing the accuracy of the proposed numerical methodology. Moreover, the experimentally and numerically calculated average surface Nusselt number of the heated inner cylinder for various rotation parameters, that illustrate the heat transfer behavior of the heated inner cylinder (Figure 7) also corroborates the validity of the numerical methodology.

The variation in the average surface Nusselt number depicted in Figure 7 is incorporated with the results reported by Chithrakumar et al.[20] in the rotation parameter range $212 \leq \zeta \leq 527$.

TABLE 1 Uncertainty estimation

| | | Independent parameter | | | | | | Dependent parameter | | | | | | |
		$D_{i,o}$, d (mm)	H (mm)	T (°C)	V (V)	I (A)	N (rpm)	A (%)	Q (%)	h_{avg} (%)	Nu_{avg} (%)	Re_{Ω} (%)	Gr (%)	ζ (%)
$q'' = 80\,\mathrm{W/m^2}$	$\zeta = 527$	0.01	1.0	0.20	0.10	0.01	1.0	0.16	2.2	2.4	2.6	2.1	1.4	0.65
	$\zeta = 1190$	0.01	1.0	0.20	0.10	0.01	1.0	0.16	2.2	2.1	2.3	2.2	1.9	0.87

TABLE 2 Grid independence study ($\eta = 0.614$, $q = 80 \, \text{W/m}^2$)

Rotation parameter ζ	Heated inner cylinder average surface temperature numerically estimated for various grid sizes (K)				
976	610,574	1,222,464	**2,865,584**	**5,995,934**	10,092,434
	320.21	318.12	**315.28**	**315.18**	315.16
2217	319.75	318.15	**316.23**	**315.15**	315.18
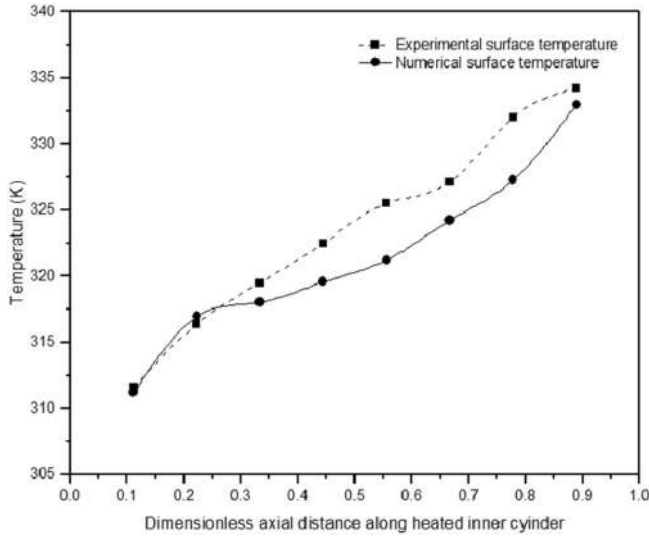
FIGURE 6 Experimental and numerical surface temperature comparison, $\zeta = 743$
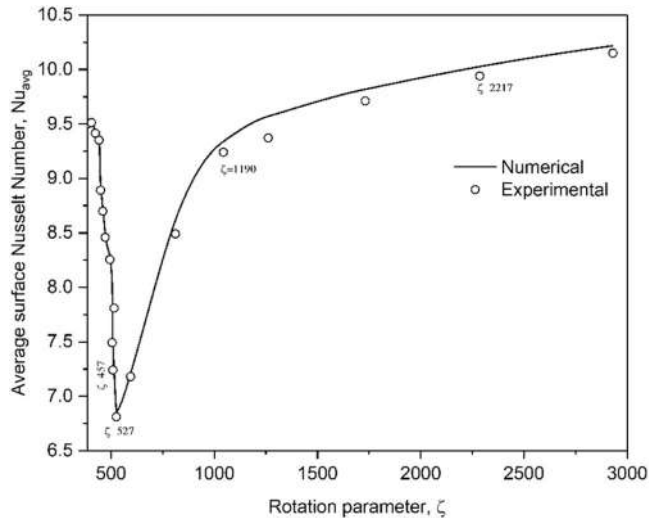
FIGURE 7 Nusselt number variation with rotation parameter, ζ

This exercise was done to show that the thermal performance of the heated inner cylinder showed deterioration in the rotation parameter range $212 \leq \zeta \leq 527$ before showing an increase in the range $527 \leq \zeta \leq 2860$. The reason for the deterioration in heat transfer in the aforementioned rotation parameter has already been detailed by Chithrakumar et al.

It is evident from Figure 7 that as the rotation parameter is increased in the range $527 \leq \zeta \leq 1190$, a sharp increase in heat transfer was observed. However, since $\zeta = 1190$ and thereafter up to $\zeta \leq 2860$ only marginal improvement in heat transfer was observed. This conundrum in the thermal behavior of the heated inner cylinder is elucidated based on the information gathered from the flow field obtained from the numerical simulations. It is well-documented in the literature pertaining to turbulent flow[39,40] that the influence of vortical structures on heat transfer could be explained based on the turbulent kinetic energy (TKE) near the heated cylinder and convective mass flow through the annulus. The influence of axial mass flow rate on heat transfer rate in the annulus is also documented in the literature by many authors.[21,22,41]

Figure 8 depicts the variation in TKE along the annular height at a dimensionless radial distance located within the turbulent thermal boundary layer. To ensure that the selected dimensionless distance is within the turbulent boundary layer, the dimensionless temperature across the annular gap was plotted for rotation parameter $\zeta = 976$ at eight points located equidistantly along the annular height as delineated in Figure 9 (similar observations were made for other rotation parameters but not shown here for conciseness). This exercise gave us an idea about the approximate dimensions of the thermal boundary layer. It is evident that the thermal boundary layer can be located along the heated inner cylinder within 10% of the annular gap width. This ensured that the radial distance considered for the TKE plot was located well within the thermal boundary layer. Also, the data pertaining to the mass flow rate through the annulus was obtained from the simulation and is illustrated in Table 3.
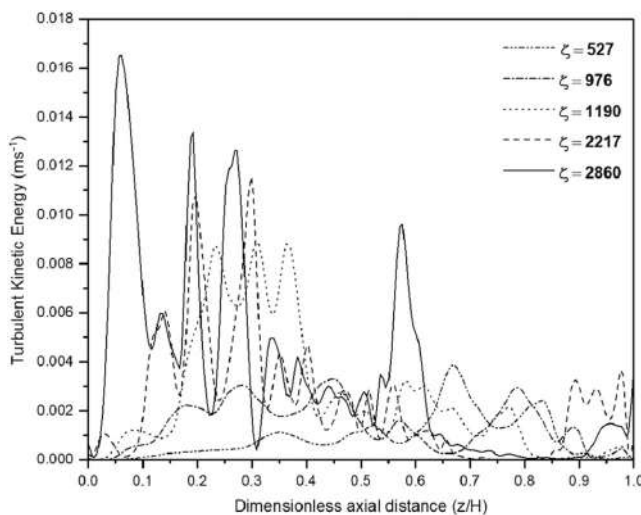

FIGURE 8 Average turbulent kinetic energy distribution along the height of the annulus at $\frac{r - r_i}{r_0 - r_i} = 0.01$
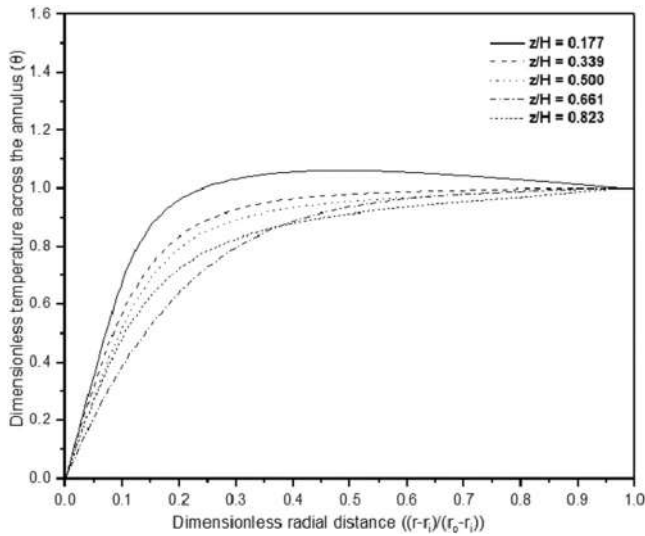
FIGURE 9 Dimensionless radial temperature distribution along different heights of the annulus

TABLE 3 Average mass flow rate ($\eta = 0.614$, $q = 80\,\text{W/m}^2$)

Mass flow rate ($\times 10^{-6}$) kg/min	Rotation parameter ζ					
$\dot{m}$	527	527	976	1190	2217	2860
	5.79	5.79	5.13	4.79	3.12	2.84

It can be seen from Figure 8, that as the rotation parameter is increased from $\zeta = 527$ to $\zeta = 1190$ the TKE near the heated stationary inner cylinder increases resulting in improved heat transfer. However, this is associated with a continuous decrease in the mass flow rate as evident from Table 3. To understand this, the variation in magnitude of axial and radial velocities at various rotation parameters as depicted in Figure 10 is considered. As the rotational speed increases, the axial velocity decreases in magnitude whereas the radial component of velocity increases. This signifies that the centrifugal forces are dominating the flow field, and significantly modifying the flow field velocities.

As the centrifugal forces increase, the flow in the radial direction increases resulting in the formation of vortical structures in the vertical plane as evident from the streamline plots in the vertical plane (Figures 11–15). These vortices may be spiral vortices and as the rotational speed increases, the increased centrifugal forces finally result in the formation of eddies in the horizontal plane as well as innately entrapping the fluid within the annulus (Figure 15). This significantly reduces the mass flow rate through the annulus as clearly evident from Table 3.

Even though the decrease in mass flow rate can result in deterioration in heat transfer, a steep improvement in heat transfer is observed for $527 \leq \zeta \leq 1190$ (Figure 7). This is attributed to the formation of vortical structures adjacent to the stationary inner cylinder as evident from the streamline plots shown in Figures 11–13. When the rotation parameter is increasing to $\zeta = 527$, these vortices are predominantly focused on the rotating outer cylinder away from the heated inner cylinder.
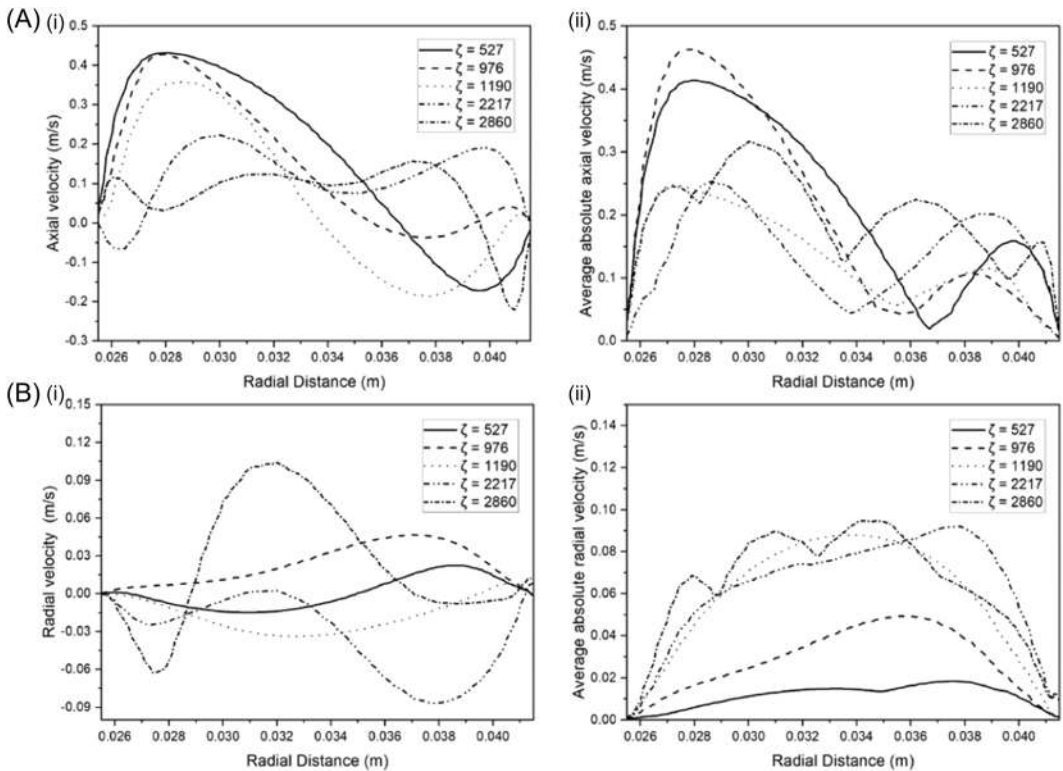
FIGURE 10 Variation in velocity and absolute velocities (i and ii) across the annular gap (A) in the axial direction; (B) in the radial direction

Further increase in rotation parameter from $\zeta = 1190$ to $\zeta = 2860$ showed only a marginal improvement in heat transfer (Figure 7) even though a steady increase in TKE was observed near the heated inner cylinder (Figure 8). This may be attributed to the steady significant fall in mass flow rate through the annulus. The strong centrifugal force developed within the annulus results in entrapping the fluid within the annulus. The entrapped fluid recirculates within the annulus as evident from the increase in the number and size of the vortices near the heated inner cylinder (Figures 14 and 15). This further results in a substantial decrease in annular mass flow rate as evident from Table 3.

The influence of dominated centrifugal force on heat transfer and mass flow rate in the annulus can be understood by monitoring the isotherm pattern[42,43] within the annulus (Figure 16). As evident from the figure, the increase in TKE resulted in the redistribution of the temperature field within the annulus from parallel vertical lines at lower speeds to horizontal uneven lines at higher values. This leads to a drop in the heat capacity rate of the fluid. To get a quantitative insight into this decrease in heat transfer, the temperature variation across the annulus was plotted at different dimensionless annular heights. Figures 17–19 depict this variation in temperature across the annulus for rotation parameters $\zeta = 1190$, 2217, and 2860, respectively. It can be inferred from these figures that as the rotation parameter increases, the temperature gradient across the thermal boundary layer decreases by 5.7°C, 4.5°C, and 3.5°C, respectively, for the above-mentioned rotation parameters. Also, it is evident from the above
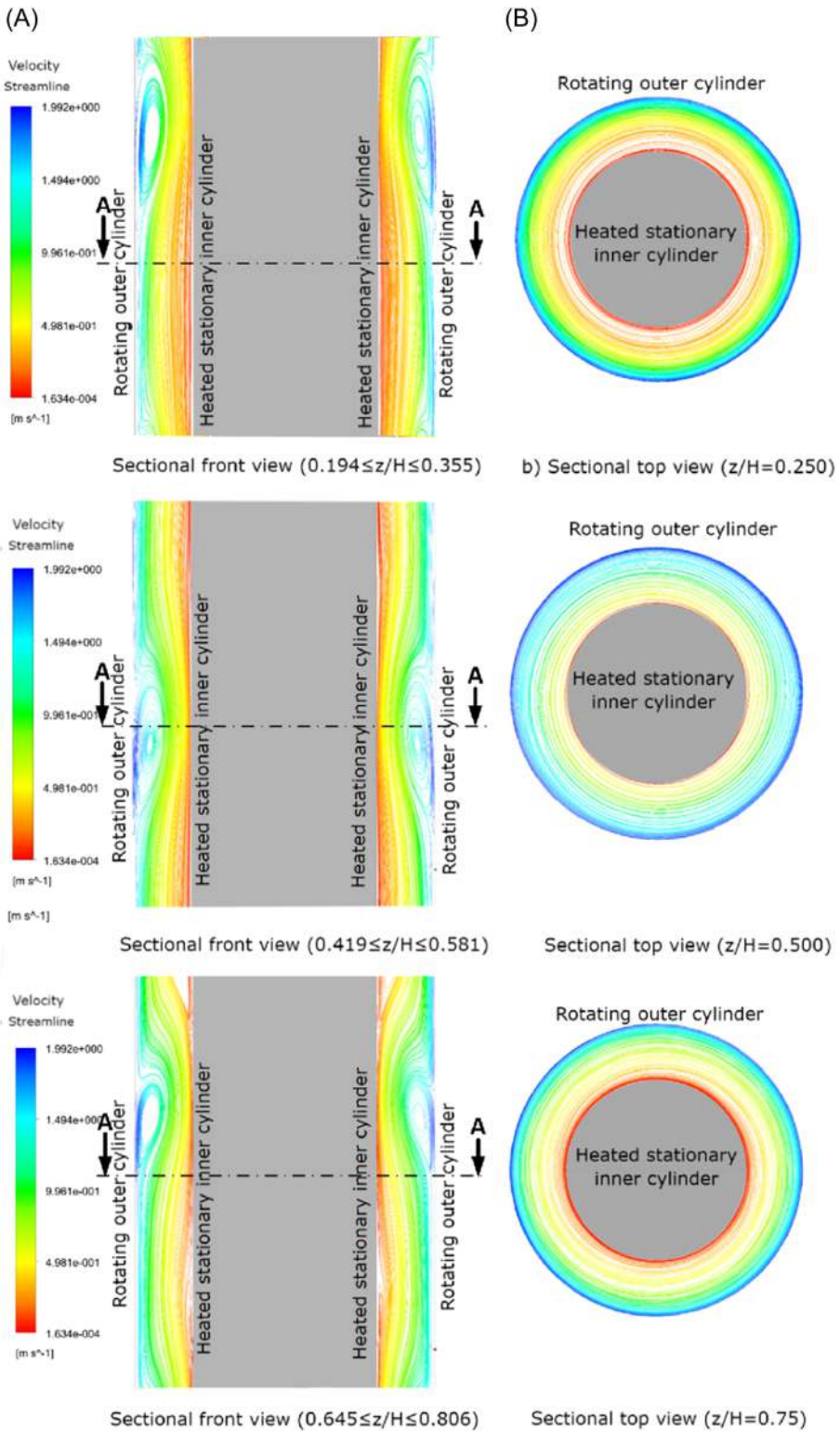
FIGURE 11 Streamlines for rotation parameter ($\zeta = 527$) [Color figure can be viewed at wileyonlinelibrary.com]
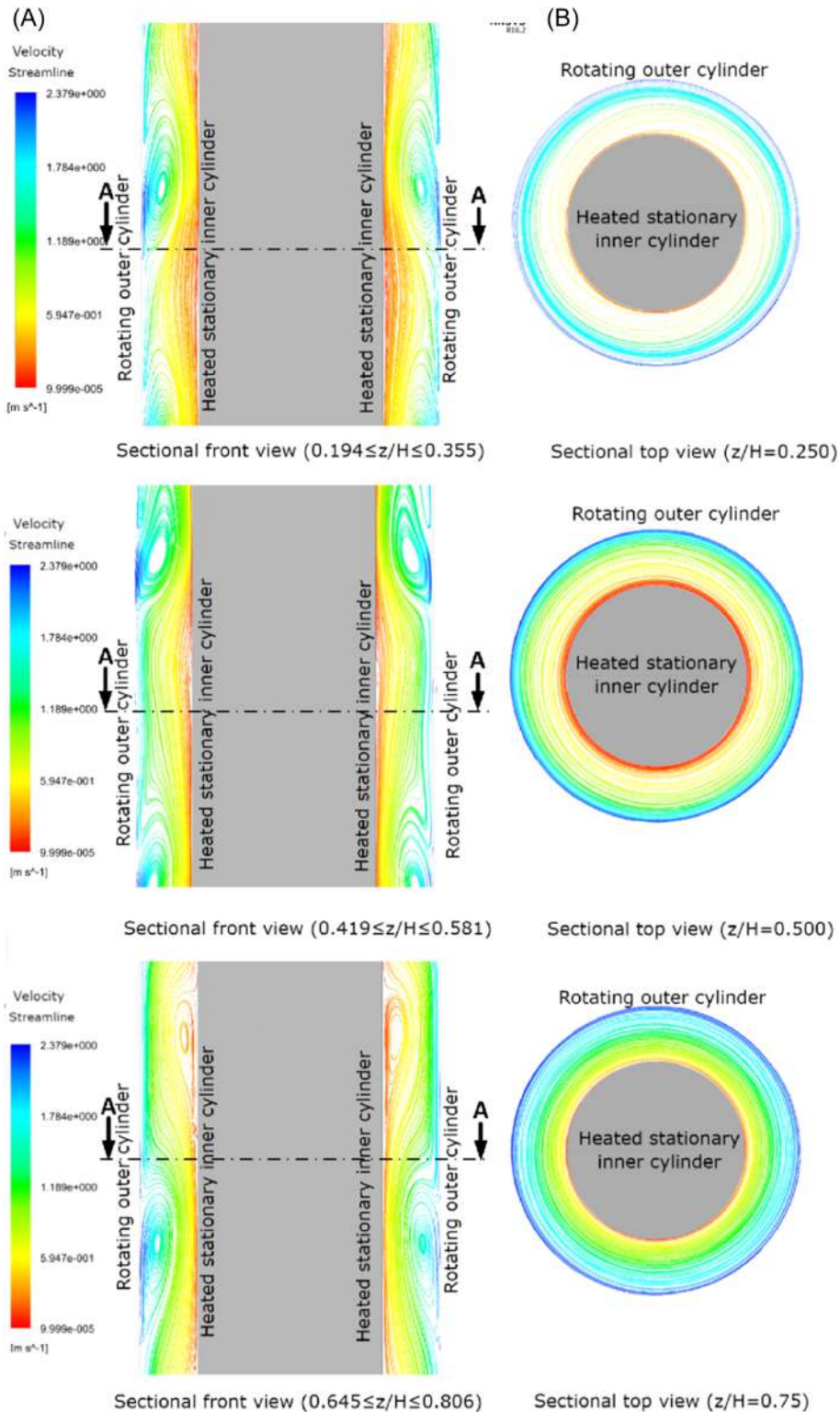
FIGURE 12 Streamlines for rotation parameter ($\zeta = 976$) [Color figure can be viewed at wileyonlinelibrary.com]
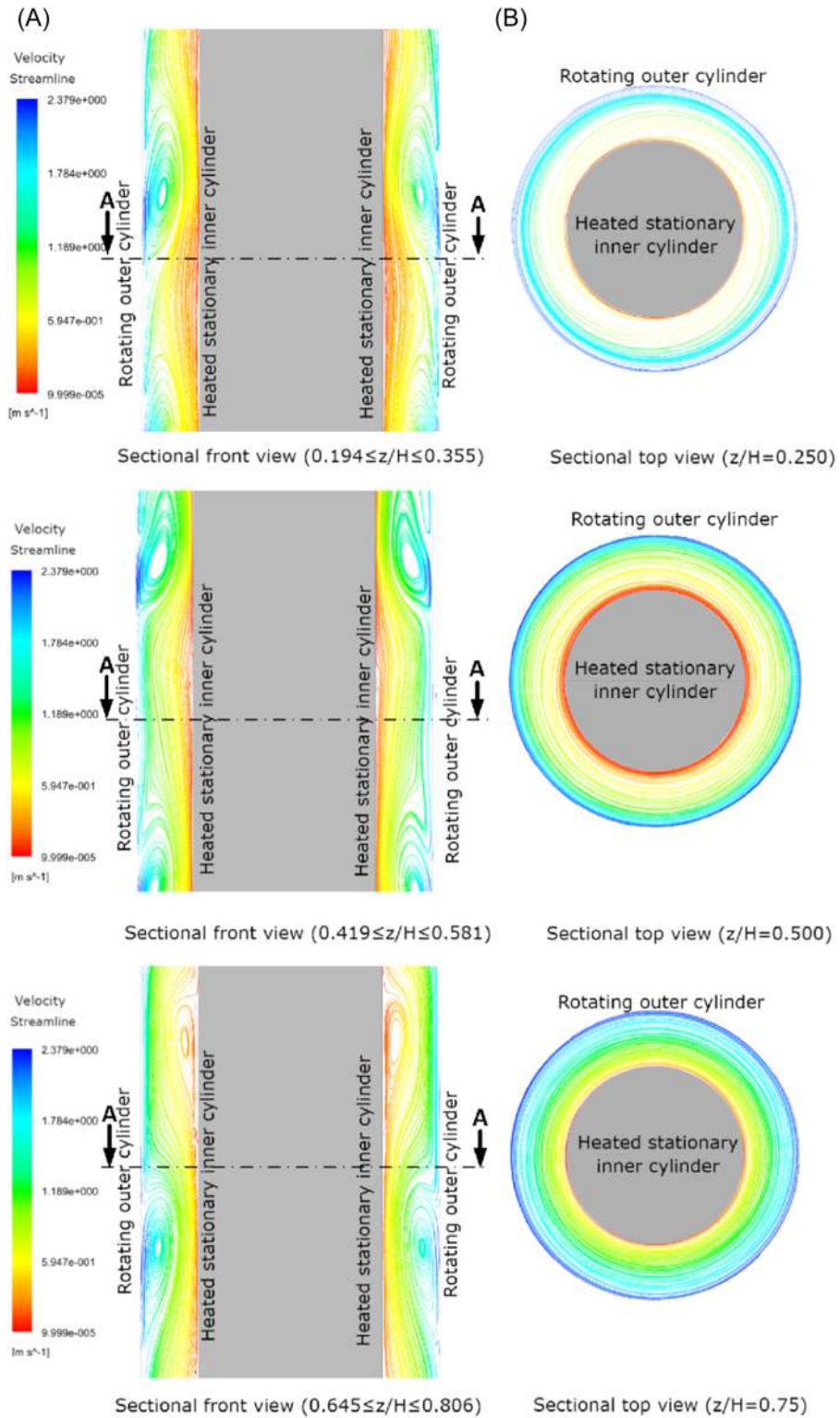
FIGURE 13 Streamlines for rotation parameter ($\zeta = 1190$) [Color figure can be viewed at wileyonlinelibrary.com]
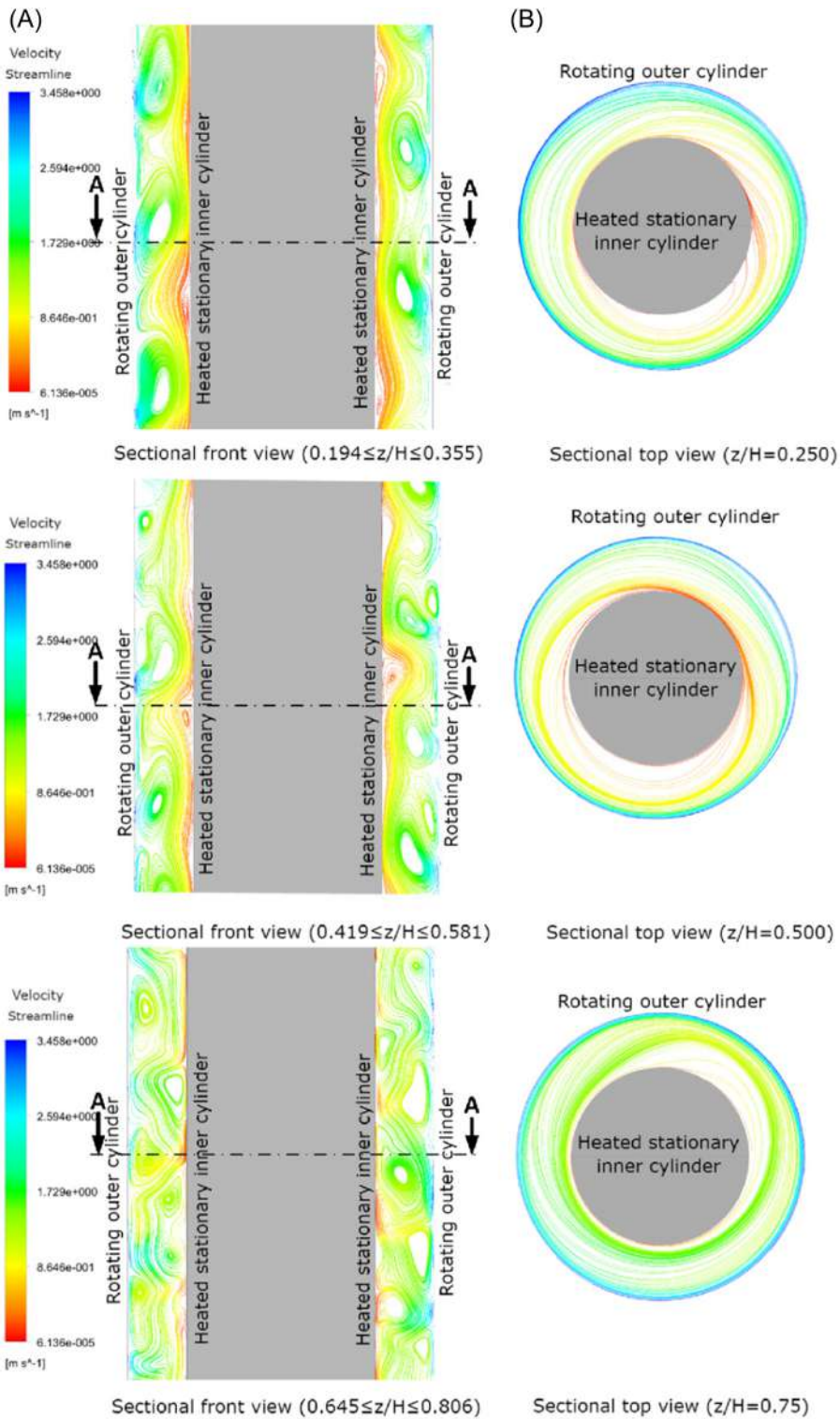
FIGURE 14 Streamlines for rotation parameter ($\zeta = 2217$) [Color figure can be viewed at wileyonlinelibrary.com]
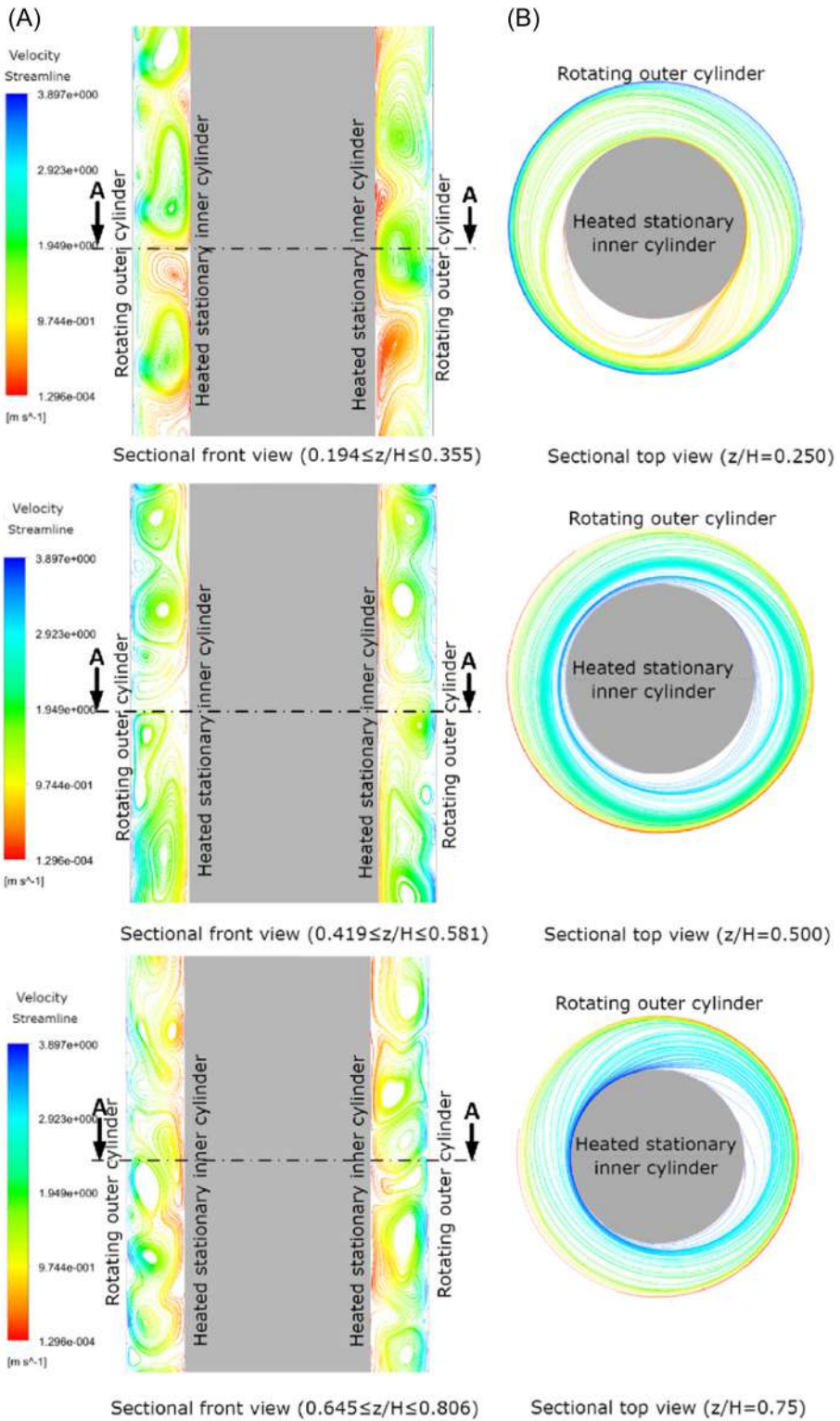
FIGURE 15 Streamlines for rotation parameter ($\zeta = 2860$) [Color figure can be viewed at wileyonlinelibrary.com]
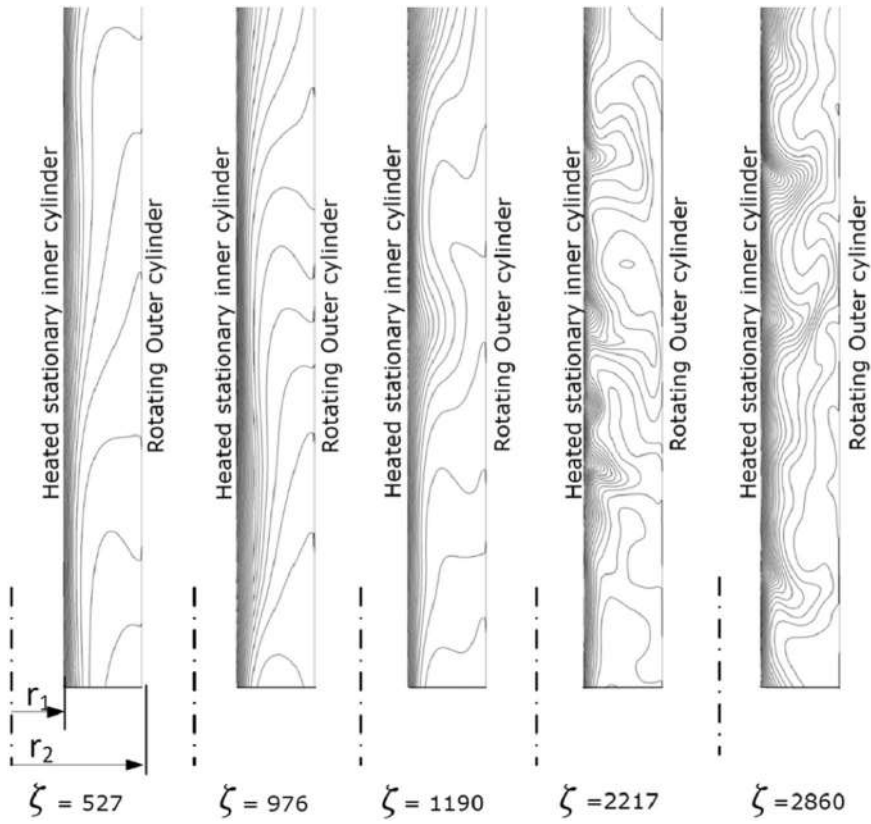
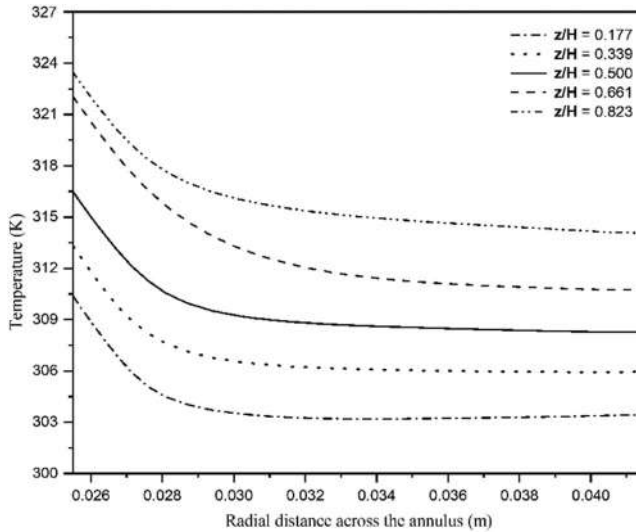**FIGURE 16**   Isotherms in vertical plain $\left(0.564 \leq \frac{z}{H} \leq 0.726\right)$

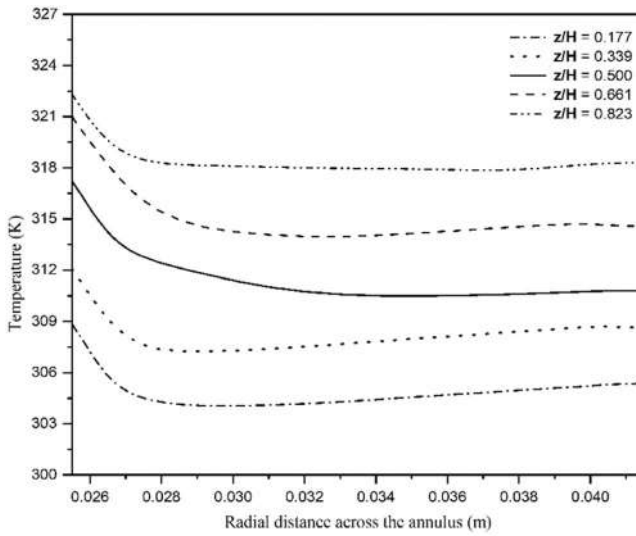**FIGURE 17**   Temperature across the annulus $(\zeta = 1190)$

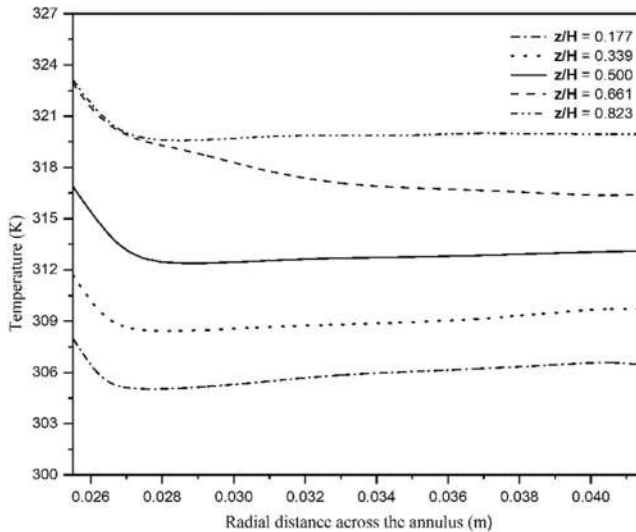**FIGURE 18** Temperature across the annulus ($\zeta = 2217$)

FIGURE 19 Temperature across the annulus ($\zeta = 2860$)

figures that the absolute temperature of the bulk fluid within the annulus increases. This is a clear indication of the degradation of the heat capacity rate of fluid that affects heat transfer from the heated inner cylinder.

Thus, at higher rotational speed, the combined effect of decreased mass flow rate due to flow entrapment and increased TKE near the heated inner cylinder results in only a marginal improvement in heat transfer. Hence we can conclude that the influence of the speed of rotation of the outer cylinder on natural convection heat transfer from the inner cylinder becomes limited at higher rotational speeds of the outer cylinder. This urges us to look into

other options like fins, grooves, or other alternative approaches that could modify the flow field for an improvement in heat transfer.

6 | CONCLUSION

The impact of higher rotational speeds of the outer cylinder on convective heat transfer in a vertical annulus with a stationary heated inner cylinder was studied both experimentally and numerically. The important conclusions from the study are as follows:

- Heat transfer from the stationary heated inner cylinder showed significant improvement as the rotation parameter was increased from $527 \leq \zeta \leq 1190$.
- The augmentation in heat transfer in the above-mentioned rotation parameter range ($527 \leq \zeta \leq 1190$) can be attributed to the formation of turbulent structures towards the heated stationary inner cylinder with an associated decrease in mass flow rate.
- However, in the rotation parameter range $1190 \leq \zeta \leq 2860$, a marginal improvement in heat transfer was observed even though there was a significant improvement in the TKE.
- This heat transfer behavior could be attributed to the significant reduction in mass flow rate that subsequently resulted in devaluation in the heat carrying capacity rate of the bulk fluid.
- In the rotational parameter range $1190 \leq \zeta \leq 2860$, the devaluation in heat capacity rate of the fluid is attributed to the formation of vortical structures in the horizontal plane of the annulus as is apparent from the streamline plots.

NOMENCLATURE

A	heated stationary inner cylinder surface area (m^2)
d	annular gap, $D_o - D_i$ (m)
g	acceleration vector due to gravity (m/s^2)
Gr	Grashof number, $\frac{g\beta\Delta T d^3}{\nu^2}$
h	heat transfer coefficient (W/m^2 K), specific enthalpy (J/kg)
H	height of the annulus (m)
k	turbulence kinetic energy (m^2/s^2)
p	pressure (Pa)
r	radial coordinate (m)
T	temperature (K)
Nu	surface Nusselt number
Pr_t	turbulent Prandtl number
Q	heat input (W)
Re_Ω	rotational Reynolds number
u_i	velocity vector (m/s)
u, v, w	axial, radial, and tangential velocity components (m/s)
z	axial coordinate (m)

GREEK SYMBOLS

Ω	angular velocity (rad/s)
θ	dimensionless temperature, $\frac{T_s - T}{T_s - T_b}$
μ	dynamic viscosity (kg/m s)

β isobaric volumetric expansivity of fluid (1/K)

η radius ratio, $\frac{r_i}{r_o}$

ζ rotation parameter, $\frac{Re_{\Omega}^2}{Gr}$

ω specific turbulence dissipation rate (m^2/s^3)

λ thermal conductivity of fluid (W/m K)

SUBSCRIPTS

a   ambient

avg average

b   bulk

d   extended domain

f   fluid

i   inner

in   inlet

o   outer

out outlet

ref reference

s   surface

t   turbulent

DATA AVAILABILITY STATEMENT

The data that support the findings of this study are available from the corresponding author upon reasonable request.

ORCID

Godson L. Asirvatham http://orcid.org/0000-0001-6323-8479

Somchai Wogwises http://orcid.org/0000-0003-2648-6814

REFERENCES

1. Taylor GI. Stability of a viscous liquid contained between two rotating cylinders. *Phil Trans R Soc Lond A.* 1923;223:289-343.

2. Gazley C. Heat transfer characteristics of the rotational and axial flow between concentric cylinders. *J Heat Transfer.* 1962;80:79-90.

3. El-Shaarawi MAI, Sarhan A. Developing laminar free convection in an open ended vertical annulus with a rotating inner cylinder. *J Heat Transfer.* 1981;103(3):552-558.

4. Fenot M, Bertin Y, Dorignac E, Lalizel G. A review of heat transfer between concentric rotating cylinders with or without axial flow. *Int J Therm Sci.* 2011;50(7):1138-1155.

5. Yoshikawa HN, Nagata M, Mutabazi I. Instability of the vertical annular flow with a radial heating and rotating inner cylinder. *Phys Fluids.* 2013;25(11):114104.

6. Guillerm R, Kang C, Savaro C, et al. Flow regimes in a vertical Taylor-Couette system with a radial thermal gradient. *Phys Fluids.* 2015;27(9):094101.

7. Sankar M, Kiran S, Ramesh GK, Makinde OD. Natural convection in a non-uniformly heated vertical annular cavity. *Defect Diffus Forum.* 2017;377:189-199.

8. Lopez JM, Marques F, Avila M. Conductive and convective heat transfer in fluid flows between differentially heated and rotating cylinders. *Int J Heat Mass Transfer.* 2015;90:959-967.

9. Schneider M, Younis BA, Weigand B. Large-eddy simulations of flow and heat transfer in heated concentric annulus with inner cylinder rotation. *Int J Heat Mass Transfer.* 2017;114:1248-1262.

10. Nouri-Borujerdi A, Nakhchi ME. Heat transfer enhancement in annular flow with outer grooved cylinder and rotating inner cylinder: review and experiments. *Appl Therm Eng*. 2017;120:257-268.

11. Lawrence JR, Swerhone GDW, Neu TR. A simple rotating annular reactor for replicated biofilm studies. *J Microbiol Methods*. 2000;42(3):215-224.

12. Kim MS, Lee KS, Um S. Numerical investigation and optimization of the thermal performance of a brushless DC motor. *Int J Heat Mass Transfer*. 2009;52(5-6):1589-1599.

13. Choi J, Lee JH, Jung YG, Park H. Enhanced efficiency of the brushless direct current motor by introducing air flow for cooling. *Heat Mass Transfer*. 2020;56:1825-1831.

14. Yoo J-S. Mixed convection of air between two horizontal concentric cylinders with a cooled rotating outer cylinder. *Int J Heat Mass Transfer*. 1998;41(2):293-302.

15. Lee JS, Xu X, Pletcher RH. Effects of wall rotation on heat transfer to annular turbulent flow: outer wall rotating. *ASME J Heat Transfer*. 2005;127:830-838.

16. Hadziabedic M, Hanjali CK, Mullyadzhanov R. LES of turbulent flow in a concentric annulus with rotating outer wall. *Int J Heat Fluid Flow*. 2013;43:74-84.

17. Ejaz MF, Manzoor S. Experimental investigation of heat transfer in a vertical annulus with a bottom heated rotating inner cylinder. *Int J Heat Technol*. 2018;36(2):730-740.

18. Mallikarjuna B, Rashad A, Hussein AK, Raju S. Transpiration and thermophoresis effects on non-Darcy convective flow past a rotating cone with thermal radiation. *Arab J Sci Eng*. 2016;41(11):4691-4700.

19. Bousbai M, Ould-Rouiss M, Mazouz A, Mataoui A. Turbulent heat transfer characteristics of water flow in a rotating pipe. *Heat Mass Transfer*. 2013;49(4):469-484.

20. Chithrakumar VK, Venugopal G, Rajkumar MR. Convection in vertical annular gap formed by stationary heated inner cylinder and rotating unheated outer cylinder. *Heat Mass Transfer*. 2019;55:2873-2888.

21. Dyko MP, Vafai K. Three-dimensional natural convective states in a narrow-gap horizontal annulus. *J Fluid Mech*. 2001;445:1-36.

22. Howell JohnR, Menguc MP, Siegel R. *Thermal Radiation Heat Transfer*. CRC Press; 2015.

23. Hussain S, Hussein AK. Mixed convection heat transfer in a differentially heated square enclosure with a conductive rotating circular cylinder at different vertical locations. *Int Commun Heat Mass Transfer*. 2011;38:263-274.

24. George WK. *Lectures in Turbulence for the 21st Century*. Chalmers University of Technology; 2013.

25. ANSYS CFX, Incor., 275,Technology Drive, Canonsburg, USA, 2006.

26. Benim AC, Nahavandi A, Syed KJ. URANS and LES analysis of turbulent swirling flows. *Prog Comput Fluid Dyn Int J*. 2005;5(8):444-454.

27. Benim AC, Escudier MP, Nahavandi A, Nickson AK, Syed KJ, Joos F. Experimental and numerical investigation of isothermal flow in an idealized swirl combustor. *Int J Numer Methods Heat Fluid Flow*. 2010;20(3):348-370.

28. Drikakis D, Rider W. *High-Resolution Methods for Incompressible and Low-Speed Flows*. 1st ed. Springer; 2005.

29. Ahlers G, Araujo FF, Funschilling D, Grossmann S, Lohse D. Non-Oberbeck–Boussinesq effects in gaseous Rayleigh–Benard convection. *Phys Rev Lett*. 2007;98(5):054501.

30. Bazdidi-Tehrani F, Moghaddam S, Aghaamini M. On the validity of Boussinesq approximation in variable property turbulent mixed convection channel flows. *Heat Transfer Eng*. 2018;39(5):473-491.

31. da Silva AK, Lorente S, Bejan A. Optimal distribution of discrete heat sources on a wall with natural convection. *Int J Heat Mass Transfer*. 2004;47:203-214.

32. Langellotto L, Manca O, Nardini S. Numerical investigation of transient natural convection in air in a convergent vertical channel symmetrically heated at uniform heat flux. *Numer Heat Transfer A*. 2007;51(11):1065-1086.

33. Rajkumar MR, Venugopal G, Anil Lal S. Natural convection with surface radiation from a planar heat generating element mounted freely in vertical channel. *Heat Mass Transfer*. 2011;47:789-805.

34. ANSYS ICEM CFD, Incor., 275,Technology Drive, Canonsburg, USA, 2006.

35. Launder BE, Spalding DB. The numerical computation of turbulent flows. *Comput Methods Appl Mech Eng*. 1974;3:269-289.

36. Moguen Y, Kousksou T, Bruel P, Vierendeels J, Dick E. Rhie-Chow interpolation for low Mach number flow computation allowing small time steps. In: Fořt J, Fürst J, Halama J, Herbin R, Hubert F, eds. *Finite Volumes for Complex Applications VI Problems and Perspectives*. Vol 4. Springer; 2011:703-711.

37. Kline SJ, McClintock FA. Describing uncertainties in single sample experiments. *Mech Eng*. 1953;75:3-8.

38. Kline SJ. The purposes of uncertainty analysis. *J Fluids Eng*. 1985;107:153-160.

39. Lowery GW, Vachon RI. The effect of turbulence on heat transfer from heated cylinders. *Int J Heat Mass Transfer*. 1975;18(11):1229-1242.

40. Ames FE. Turbulence effects on convective heat transfer. In: Kulacki F, ed. *Handbook of Thermal Science and Engineering*. Springer; 2017:1-33.

41. Dondapati RS, Rao VV. Influence of mass flow rate on turbulent kinetic energy (TKE) distribution in cable-in-conduit conductors (CICCs) used for fusion grade magnets. *Fusion Eng Des*. 2013;88(5):341-349.

42. Hussain S, Hussein AK. Numerical investigation of natural convection phenomena in a uniformly heated circular cylinder immersed in square enclosure filled with air at different vertical locations. *Int Commun Heat Mass Transfer*. 2010;37(8):1115-1126.

43. Hussein AK. Computational analysis of natural convection in a parallelogrammic cavity with a hot concentric circular cylinder moving at different vertical locations. *Int Commun Heat Mass Transfer*. 2013;46:126-133.